Propagator theory of brain dynamics

P. A. Robinson
School of Physics, University of Sydney, New South Wales 2006, Australia and Brain Dynamics Center, Westmead Hospital, Westmead, New South Wales 2145, Australia
(Received 10 November 2004; published 8 July 2005)

A physiologically based continuum model of brain dynamics is extended to incorporate arbitrary numbers of structures and neural populations, multiple outgoing fields of activity from a single population of neurons to various targets, improved treatment of converging or diverging projections and mesoscopic structure, and generalized connections to quantities observable via electroencephalography and other methods. The results are applied to study the corticothalamic system, predicting an intracortical resonance that leads to enhancements of electroencephalographic activity in the gamma (>30 Hz) range. This resonance involves feedback loops incorporating slow, short-range inhibitory fibers.

DOI: 10.1103/PhysRevE.72.011904 PACS number(s): 87.19.La, 87.10.+e

I. INTRODUCTION

Physiologically based continuum modeling of brain dynamics has progressed significantly since its inception in the 1970s [1–10]. Recent work in this area has resulted in numerous quantitatively verified predictions of brain electrical activity, including electroencephalogram (EEG) time series [11–13], spectra [10–19], coherence and correlations [20], evoked response potentials (ERPs) [12,13], and seizure dynamics [11,13]. Inversion of the model predictions has also yielded estimates of underlying physiological parameters and their variations across the brain, in different states of arousal, and disorders [11,21–23].

Despite its many successes continuum modeling is still restricted in many ways. For example (i) it has included only certain brain structures (mainly the cortex and thalamus), (ii) little mesoscopic structure, such as is involved in neural arborization, has been incorporated, and (iii) widely converging or diverging projections have not been adequately treated. In addition, (iv) it has mostly neglected anisotropies, (v) approximately periodic structures, such as those seen in the visual cortex have not been incorporated [24,25], (vi) treatment of parameter dynamics, including some details of neurotransmitter kinetics, facilitation and related processes, neuromodulator dynamics, activation systems, etc., has not been systematic, (vii) development and learning have not been incorporated, and (viii) geometry and boundary conditions are only approximate.

The purpose of this paper is to generalize our analysis to incorporate the first three of the points mentioned above (it is not feasible to address all eight in a single paper). Specifically, (i) an arbitrary number of structures and neural populations are included rather than the limited numbers considered in previous works, and (ii) the analysis enables each projection (including arborization effects) between populations to be treated separately via propagator techniques, thereby removing arbitrary implicit assumptions of equal ranges of whole classes of projections [10,11,13]. Problems that require this more general analysis include understanding the activation systems of the brain that govern arousal and attention (hence, cognitive questions, ERPs, and sleep), exploration of the mechanisms of gamma oscillations at frequencies above 30 Hz, study of the effects of the multilayered structure of the cortex, investigation of the role of structures such as the basal ganglia and limbic system in brain dynamics and disorders (Parkinson's disease, etc.), and deeper understanding of seizure dynamics.

In generalizing our earlier analysis, the main aims are to obtain a model that is tractable (especially via a formulation in terms of differential equations), backward compatible with our earlier work in appropriate limits, physiologically justifiable, and relies on parameters that are experimentally measurable.

In Sec. II we make a number of generalizations of our previous theory, as outlined above. These are based on physiological and anatomical insights, and aim for mathematical tractability in the final equations. This leads to a formulation in terms of propagators for waves of neural activity. Propagators have been used in brain dynamics contexts before (e.g., [7,14]), but not so extensively; they yield the most convenient formulation in the present case. General properties of the model are discussed in Secs. III and IV, including its steady-state behavior and linear responses. Specific illustrative applications to the corticothalamic system and generation of gamma oscillations are made in Sec. V, where an additional intracortical gamma resonance is found.

II. THEORY

In this work (and our previous ones) we make a continuum approximation in which neural properties are averaged over linear scales of a tenth of a millimeter or so: sufficient to contain large numbers of neurons, but small enough to resolve fine structures in the brain. There are several main aspects to the theory, each of which is dealt with in a subsection below, including its physiological basis: (i) synaptic and dendritic dynamics and summation of synaptic inputs to determine potentials at the neural cell body (soma), (ii) generation of pulses at the axonal hillock, and (iii) propagation of pulses within and between neural populations. In each subsection, we first formulate the relevant physics in terms of the physiology, explain the main features of the resulting equations, and discuss their limitations. We then show how

tractable differential-equation forms can be obtained, show how useful approximations can be made in certain cases, and discuss how the equations reduce to those we have introduced in previous work in the appropriate limits. Where results from a previous analysis are used directly, the full justification is not repeated here.

A. Synaptodendritic dynamics and the soma potential

We assume that the brain contains multiple populations of neurons, distinguished by a subscript a, which simultaneously labels both the structure in which a given population lies (e.g., a particular nucleus) and the type of neuron (e.g., interneuron, pyramidal cell). The continuum soma potential V_a is the sum of contributions V_{ab} arriving as a result of activity at each type of (mainly) dendritic synapse b, where b distinguishes both the incoming neural population and the neurotransmitter type of the receptor. Thus we write [17]

$$V_a(\mathbf{r},t) = \sum_b V_{ab}(\mathbf{r},t), \tag{1}$$

where $\mathbf{r}$ denotes the spatial coordinates, t the time, the summation is assumed to be linear, and all potentials are measured relative to resting [15]. For moderate perturbations relative to a steady state, the value of the reveral potential can be subsumed into the values of other parameters, by means discussed in a previous analysis [15]; more generally, it could be retained as a separate term, but we do not do so here. Geometrically, the cortex is approximated as a two-dimensional sheet and $\mathbf{r}$ is assumed to be the actual position in the case of the cortex; many other structures, such as the thalamus, are linked to the cortex via a primary topographic map, that links points in a one-to-one manner between structures; we assign the same value of $\mathbf{r}$ to such points. Hence, in structures other than the cortex, this dimensional *map coordinate* $\mathbf{r}$ denotes a *rescaled* physical dimension (i.e., the physical coordinate multiplied by the ratio of the cortical scale to the structure's scale), a point that must be remembered when considering values of spatial parameters in these structures. An alternative approach would be to rescale coordinates in each structure by dividing by its linear scale, thereby again leading to a fixed common range of $\mathbf{r}$, but dimensionless coordinates in this case. In what follows, all positions are given in dimensional map coordinate units, unless otherwise stated.

The subpotentials V_{ab} respond in different ways to incoming spikes, depending on their synaptic dynamics (ion-channel kinetics, diffusion in the synaptic cleft, etc.), and on subsequent signal dispersion in the dendrites. The resulting soma response to a δ-function input at the synapse can be approximated via the differential equation [10]

$$D_{ab}(\mathbf{r},t)V_{ab}(\mathbf{r},t) = P_{ab}(\mathbf{r},t), \tag{2}$$

$$D_{ab}(\mathbf{r},t) = \frac{1}{\alpha_{ab}(\mathbf{r},t)\beta_{ab}(\mathbf{r},t)}\frac{d^2}{dt^2} + \left[\frac{1}{\alpha_{ab}(\mathbf{r},t)} + \frac{1}{\beta_{ab}(\mathbf{r},t)}\right]\frac{d}{dt} + 1, \tag{3}$$

where P_{ab} is a weighted average number of incoming spikes arriving at $\mathbf{r}$ and t; this quantity is discussed in detail in Sec. II C. The parameter α_{ab} is the mean decay rate of the soma response to a δ-function synaptic input, while β_{ab} is the mean rise rate: this biexponential form has been widely found to be a good approximation [10,25–27].

If the α_{ab} and β_{ab} are independent of b (which is not usually true), then the subscript b on D_{ab} can be omitted and V_a itself satisfies Eq. (2) with the right side of Eq. (2) replaced by the sum of P_{ab} over b, as in most of our earlier works. This approximation is also valid if α and β are interpreted as effective values, averaged over subpopulations.

B. Pulse generation

In cells with voltage-gated ion channels, action potentials are produced at the axonal hillock in response to the soma potential exceeding some threshold θ_a. When averaged over a population of neurons with normal response characteristics, a reasonable approximation for the firing rate Q_a has been found to be

$$Q_a(\mathbf{r},t) = Q_{a\,\max} S_a[V_a(\mathbf{r},t)], \tag{4}$$

where $Q_{a\,\max}$ is the maximum firing rate due to normal channels and S_a is a monotonically increasing function that approaches zero as $V_a \to -\infty$ and unity as $V_a \to \infty$. A commonly used approximation is

$$S_a[V_a(\mathbf{r},t)] = \frac{1}{1+\exp[-\{V_a(\mathbf{r},t) - \theta_a(\mathbf{r},t)\}/\tilde{\sigma}_a(\mathbf{r},t)]}, \tag{5}$$

where θ_a is the firing threshold for channels of type a and $\sigma_a = \tilde{\sigma}_a \pi/\sqrt{3}$ is the population standard deviation of the threshold.

C. Propagation

Spatiotemporal propagation of pulses within and between populations determines the values of P_{ab} in Eq. (2) based on the values of Q_b at other locations and earlier times. This is a key area where we generalize the model by differentiating between propagators linking different structures, and including axonal and dendritic arborization.

1. Propagator formulation

If we assume linear propagation, we can write $P_{ab}(\mathbf{r},t)$ in terms of an integral over a propagator $\Lambda_{ab}(\mathbf{r},t;\mathbf{r}',t')$ for propagation of activity with the source $Q_b(\mathbf{r}',t')$:

$$P_{ab}(\mathbf{r},t) = \int \Lambda_{ab}(\mathbf{r},t;\mathbf{r}',t')Q_b(\mathbf{r}',t')d\mathbf{r}'dt'. \tag{6}$$

The propagator incorporates propagation within axons of the population b, then transfer to population a via dendritic trees. Propagators have been used in some instances in brain dynamics contexts, particularly in the study of the effects of volume conduction on signals reaching the scalp from the brain [7], and in an earlier paper on gamma oscillations [14], which used an insufficiently detailed physiological model, and did not distinguish sufficiently between all the projections originating from a given neural population.

We can rewrite Eq. (6) in the form

$$P_{ab}(\mathbf{r},t) = \int \Delta_a(\mathbf{r},t;\mathbf{r}'',t'')\tilde{\Gamma}_{ab}(\mathbf{r}'',t'';\mathbf{r}',t') \times Q_b(\mathbf{r}',t')d\mathbf{r}''dt''dr'dt'; \quad (7)$$

here, $\tilde{\Gamma}_{ab}$ governs propagation within population b from the source to the point $\mathbf{r}'',t''$ of a synapse with population a, while Δ_a governs the subsequent propagation along connections between the populations, including along the dendritic trees of cells a to a soma location $\mathbf{r},t$.

The index a in Eqs. (6) and (7) includes all populations whose activity can be affected by incoming stimuli. For inputs of external stimuli Q_b the index b can also label stimulus types (e.g., left and right eye, color, etc., with a separate value of b for each type of stimulus). This separation of stimuli into subtypes is necessary to allow for competition in development and learning, but can be dispensed with in applications where this distinction is not relevant. This split does not incorporate feedback from the brain to the sensory cells, but such an effect could easily be included by treating all nervous system structures on the same formal footing. Noise inputs to all neural populations can also be included via this approach, to model either random external stimuli or statistical fluctuations in spike rate.

A useful form of Eq. (7) is obtained by incorporating the spatial spread of the function Δ_a into a factor Γ_{ab} that also includes the spatial propagation implicit in $\tilde{\Gamma}_{ab}$, while keeping information on discrete time delays $\tau_{ab}(\mathbf{r},t)$ between remotely situated populations separate from a local coupling-strength factor ν_{ab}. This yields

$$P_{ab}(\mathbf{r},t) = \nu_{ab}(\mathbf{r},t)\int \delta(t-t'')\delta[t''-t'-\tau_{ab}(\mathbf{r},\mathbf{r}',t)] \times \Gamma_{ab}(\mathbf{r},t'';\mathbf{r}',t')Q_b(\mathbf{r}',t')dt''d\mathbf{r}'dt' \quad (8)$$

$$= \nu_{ab}(\mathbf{r},t)\int \delta[t-t'-\tau_{ab}(\mathbf{r},\mathbf{r}',t)] \times \Gamma_{ab}(\mathbf{r},t;\mathbf{r}',t')Q_b(\mathbf{r}',t')d\mathbf{r}'dt' \quad (9)$$

$$= \nu_{ab}(\mathbf{r},t)\phi_{ab}[\mathbf{r},t-\tau_{ab}(\mathbf{r},\mathbf{r}',t)] \quad (10)$$

$$= \nu_{ab}(\mathbf{r},t)\eta_{ab}(\mathbf{r},t), \quad (11)$$

where comparison of Eqs. (9) and (10) defines the pulse density field ϕ_{ab} that comprises signals from population b to a. Thus, the dimensionality of the integration has been halved, from 6 to 3, and the nonlocal form of Δ_a has been replaced by the simpler, local ν_{ab}, at the cost of introducing additional propagators to incorporate the different degrees of convergence and divergence. Equation (10) encapsulates propagation from soma location to soma location of a field generated immediately by Q_b but impinging on the target population a only after a delay τ_{ab}. The alternate form (11) pictures the influence of Q_b generating the field η_{ab} at the target only after the delay τ_{ab}. The latter picture is more compact for numerical implementation involving N populations because it requires storage only of N fields Q_b, rather than the N^2 fields ϕ_{ab}, during the delay τ_{ab}.

A reasonable approximation for the propagator Γ_{ab} is to retain the same form as the axonal propagator $\tilde{\Gamma}_{ab}$, but to modify the effective range r_b of the propagator to account for it now incorporating both the coordinate divergence h_{ab} of axons traveling from b to a and the extent of arborization d_a of dendritic trees of type a, giving an approximate range

$$r_{ab} = (h_{ab}^2 + d_a^2)^{1/2}. \quad (12)$$

(Note that this quantity is expressed in map coordinate units at the target population a.) These results contrast with the analyses in our previous works (cited in Sec. I), in which the propagation (and, hence, Γ_{ab} in the propagator notation used in the present work) was assumed to have the same form for all a for given b—a good approximation for intracortical propagation, but not as accurate for corticothalamic projections, for example, which are less divergent [28].

The function ν_{ab} can be written

$$\nu_{ab}(\mathbf{r},t) = N_{ab}(\mathbf{r},t)s_{ab}(\mathbf{r},t), \quad (13)$$

where N_{ab} is the mean number of connections from cells of type b per cell of type a and s_{ab} is their mean strength.

One very important point is that the arborization, divergence, and range above are measured in coordinate units, not physical lengths: these are equal only for the cortex, with a scale factor for other structures.

2. Propagators and wave equations

The propagator Γ_{ab} in Eq. (9) incorporates propagation within a population as well as additional spreading due to convergence and divergence of connections between populations. To a reasonable approximation, we treat the latter as modifying the characteristic range of the former, via Eq. (13).

A substantial body of work has shown that, to a good approximation, signals propagate within a population as if governed by a damped wave equation and, hence, that a wave propagator can be used [7,10–13,15,16,21]. This has the major advantage of enabling the propagation of ϕ_{ab} to be treated in differential form, rather than via the integral equation (9).

For an isotropic damped wave equation of the form

$$\left[\frac{1}{\gamma_{ab}^2}\frac{\partial^2}{\partial t^2} + \frac{2}{\gamma_{ab}}\frac{\partial}{\partial t} + 1 - r_{ab}^2\nabla^2\right]\phi_{ab}(\mathbf{r},t) = Q_b(\mathbf{r},t), \quad (14)$$

we find

$$\left[\frac{1}{\gamma_{ab}^2}\frac{\partial^2}{\partial t^2} + \frac{2}{\gamma_{ab}}\frac{\partial}{\partial t} + 1 - r_{ab}^2\nabla^2\right]\eta_{ab}(\mathbf{r},t) = Q_b[\mathbf{r},t-\tau_{ab}(\mathbf{r},t)], \quad (15)$$

where $\gamma_{ab}=v_{ab}/r_{ab}$ is the temporal damping coefficient and v_{ab} is the wave velocity in coordinate units. Equation (14) is also satisfied if ϕ_{ab} is replaced by $\Gamma_{ab}^{(0)}(\mathbf{r}-\mathbf{r}',t-t')$ and the right side is replaced by a source of the form $\delta(\mathbf{r}-\mathbf{r}')\delta(t-t')$. This gives

$$\Gamma_{ab}^{(0)}(\mathbf{k},\omega) = \frac{1}{(k^2 + q_{0ab}^2) r_{ab}^2}, \tag{16}$$

$$q_{0ab}^2 r_{ab}^2 = (1 - i\omega/\gamma_{ab})^2. \tag{17}$$

Equation (15) emphasizes the more compact implementation possible if η_{ab} is used in place of ϕ_{ab} in numerical calculations. Fourier transformation of Eq. (16) yields the coordinate-space propagator, while its reciprocal is the dispersion operator, which is also obtainable by Fourier transforming the contents of the square brackets in Eq. (14) directly.

Significantly, the form (16) enables very diffuse (i.e., not topographically specific) connections between populations to be handled straightforwardly, simply by increasing r_{ab} while reducing γ_{ab}, thereby allowing influences to propagate long distances with little damping. When computing γ_{ab} for propagation between remote populations, one must be careful to allow for the actual geometry of the axonal tree, a point to which we return in the Appendix.

3. Parameters

The above equations contain a number of parameters of physiology and anatomy. In general, these can vary in both space and time; however, we restrict the analysis here to spatial variations. This does not preclude treatment of temporal variations on time scales much longer than those of variations in neural activity. Specific values for one model are discussed in Sec. V and the Appendix.

III. STEADY STATES AND GLOBAL DYNAMICS

Previous work has shown that a great variety of properties of brain electrical activity can be obtained by treating activity changes as being perturbations of a steady state [11,21]. Spatially uniform steady states can be obtained by solving the preceding equations with all time and space derivatives set to zero, assuming that the parameters are spatially constant. (Spatially nonuniform steady states are also possible, and of significant interest, but we do not consider them here.) The spatially uniform steady states are thus the solutions of the set of equations

$$Q_a = S_a\left(\sum_b \nu_{ab} Q_b\right), \tag{18}$$

which are generally transcendental in form. Partial derivatives of the solutions of Eq. (18) with respect to the parameters can be used to probe their zero-frequency stability, and to help determine the most suitable control parameters for state modification.

Much of the dynamics of brain electrical activity occurs at relatively large spatial scales, and the largest scales are often the least stable (and, hence, the most active) [10,11]. Global dynamics can be probed in the uniform-parameter case by assuming that all the parameters are spatially constant and setting all spatial derivatives in the equations of Sec. II to zero. This enables the time derivatives to be replaced by ordinary derivatives, yielding a set of ordinary delay differential equations for the global activity. Such equations have proved useful for studying the dynamics of generalized epileptic seizures; for example [11].

IV. LINEAR AND COUPLED-MODE PROPERTIES

We can study many properties of brain activity by linearizing the equations of Sec. II around an assumed steady state. Here we allow for coupling of uniform-medium modes via spatial variations of the model parameters. We do *not* assume that the activity is uniform or constant.

A. Linear equations for activity

Of the relevant equations in Sec. II, Eqs. (1), (2), (9), and (14) or (15) are already linear. Equation (4), which is needed to close the set, can be linearized by replacing the sigmoid S_a by its slope ρ_a at the assumed steady state value of V_a. If we Fourier transform the resulting set of linear (in the fields) equations in time, we find for the fluctuating parts

$$Q_a(\mathbf{r},\omega) = \rho_a(\mathbf{r}) V_a(\mathbf{r},\omega), \tag{19}$$

$$V_a(\mathbf{r},\omega) = \sum_b V_{ab}(\mathbf{r},\omega), \tag{20}$$

$$V_{ab}(\mathbf{r},\omega) = L_{ab}(\mathbf{r},\omega) P_{ab}(\mathbf{r},\omega), \tag{21}$$

$$L_{ab}(\mathbf{r},\omega) = [1 - i\omega/\alpha_{ab}(\mathbf{r})]^{-1}[1 - i\omega/\beta_{ab}(\mathbf{r})]^{-1}, \tag{22}$$

$$P_{ab}(\mathbf{r},\omega) = \nu_{ab}(\mathbf{r}) e^{i\omega\tau_{ab}(\mathbf{r})} \phi_{ab}(\mathbf{r},\omega), \tag{23}$$

$$\phi_{ab}(\mathbf{r},\omega) = \int d\mathbf{r}' \Gamma_{ab}(\mathbf{r} - \mathbf{r}', \omega) Q_b(\mathbf{r}', \omega), \tag{24}$$

where we have assumed that all the parameters of the equations (but not the fields of activity) are constant on the time scales of interest. The spatial dependence of the parameters in Eqs. (19)–(24) couples the modes of the uniform-parameter system in a manner similar to quantum time-independent perturbation theory [17].

For any given $\mathbf{r}$ and ω, the above linear equations can be rearranged to obtain

$$Q_a(\mathbf{r},\omega) = \sum_b J_{ab}(\mathbf{r},\omega) \int d\mathbf{r}' \Gamma_{ab}(\mathbf{r} - \mathbf{r}', \omega) Q_b(\mathbf{r}', \omega), \tag{25}$$

$$J_{ab}(\mathbf{r},\omega) = L_{ab}(\mathbf{r},\omega) G_{ab}(\mathbf{r}) e^{i\omega\tau_{ab}(\mathbf{r})}, \tag{26}$$

where the gains are defined by $G_{ab}(\mathbf{r}) = \rho_a(\mathbf{r})\nu_{ab}(\mathbf{r})$.

If we spatially Fourier transform Eq. (25), we find the two equivalent convolutions

$$Q_a(\mathbf{k},\omega) = \sum_b \int \frac{d\mathbf{q}}{(2\pi)^2} J_{ab}(\mathbf{q},\omega) \Gamma_{ab}^{(0)}(\mathbf{k} - \mathbf{q}, \omega) \times Q_b(\mathbf{k} - \mathbf{q}, \omega), \tag{27}$$

$$= \sum_b \int \frac{d\mathbf{q}}{(2\pi)^2} J_{ab}(\mathbf{k}-\mathbf{q},\omega)\Gamma_{ab}^{(0)}(\mathbf{q},\omega) \times Q_b(\mathbf{q},\omega). \quad (28)$$

The existence of the primary topographic mapping is critical to obtaining the two equivalent forms (27) and (28), since it allows us to parametrize all the populations in terms of a single position coordinate and wave vector (it does not, however, require connections to be topographically one to one). Rescaling of the position vector is necessary to obtain dimensional physical locations in a given population. If the J_{ab} are independent of position, only $\mathbf{q}=\mathbf{0}$ need be included in Eq. (27), or $\mathbf{q}=\mathbf{k}$ in Eq. (28) [i.e., $J_{ab}(\mathbf{q},\omega) = (2\pi)^2 J_{ab}(\omega)\delta(\mathbf{q})$], which yields

$$Q_a(\mathbf{k},\omega) = \sum_b J_{ab}(\omega)\Gamma_{ab}^{(0)}(\mathbf{k},\omega)Q_b(\mathbf{k},\omega), \quad (29)$$

where the redundant argument has been omitted in $J_{ab}(\omega)$, which has the same dimensions as $J_{ab}(\mathbf{k},\omega)d\mathbf{q}$.

Returning to the spatially dependent case, we can replace the integral over $\mathbf{q}$ in Eq. (28) by a sum over discrete $\mathbf{q}$, to arbitrary accuracy, yielding

$$\sum_{b\mathbf{q}} \delta_{ab}\delta_{\mathbf{kq}}Q_b(\mathbf{q},\omega) = \sum_{b\mathbf{q}} C_{ab}(\mathbf{k},\mathbf{q},\omega)Q_b(\mathbf{q},\omega), \quad (30)$$

$$C_{ab}(\mathbf{k},\mathbf{q},\omega) = J_{ab}(\mathbf{k}-\mathbf{q},\omega)\Gamma_{ab}^{(0)}(\mathbf{q},\omega). \quad (31)$$

If there are N' neural populations in the system being considered, and J stimulus sources, and we assume that there is no feedback of stimuli on themselves or of the brain on stimuli (as discussed in Sec. II C 1), then the matrix $\mathbf{C}$ is $(N'+J)\times(N'+J)$ in size, but the bottom J rows are zero. Hence, Eq. (30) can be written in the form

$$\sum_{b\mathbf{q}} A_{ab}(\mathbf{k},\mathbf{q},\omega)Q_b(\mathbf{q},\omega) = \sum_{j\mathbf{q}} B_{aj}(\mathbf{k},\mathbf{q},\omega)N_j(\mathbf{k},\omega), \quad (32)$$

$$A_{ab}(\mathbf{k},\mathbf{q},\omega) = \delta_{ab}\delta_{\mathbf{kq}} - C_{ab}(\mathbf{k},\mathbf{q},\omega), \quad (33)$$

and $B_{aj}(\mathbf{k},\mathbf{q},\omega) = C_{aj}(\mathbf{k},\mathbf{q},\omega)$, where b denotes neural populations, j denotes external stimulus types, and N_j has been used in place of Q_j for the J stimulus types to make the distinction between population firing rates and incoming stimulus pulse rates absolutely clear. The matrix $\mathbf{A}$ is $N'\times N'$ in size, while $\mathbf{B}$ has N' rows and J columns; the column matrix $\mathbf{N}$ has J elements, while the remaining column matrix $\mathbf{Q}$ now has N' elements. In the case that only $\mathbf{q}=\mathbf{k}$ is retained, the eigenmodes are spatially uniform and independent, and Eqs. (30) and (31) become

$$\sum_b A_{ab}(\mathbf{k},\omega)Q_b(\mathbf{k},\omega) = \sum_j B_{aj}(\mathbf{k},\omega)N_j(\mathbf{k},\omega), \quad (34)$$

$$A_{ab}(\mathbf{k},\omega) = \delta_{ab} - C_{ab}(\mathbf{k},\omega), \quad (35)$$

$$B_{ab}(\mathbf{k},\omega) = J_{ab}(\omega)\Gamma_{ab}^{(0)}(\mathbf{k},\omega), \quad (36)$$

where the factors in Eq. (36) are defined in Eqs. (16) and (26).

It is useful to write Eq. (32) in matrix notation. To do this, one must establish a one-dimensional ordering of b and $\mathbf{k}$ or $\mathbf{q}$ to use to label the rows and columns. Discussion of how to order the spatial modes for one- (1D) and two-dimensional (2D) coordinate spaces was given elsewhere [17]. If there are N' populations, J stimulus sources, and wave number modes are truncated to run from $-M_{\max}$ to $M_{\max}$ in each dimension, then in 2D, the mode with wave vector (in a rectangular topology with periodic boundary conditions)

$$\mathbf{k} = \left(\frac{2\pi m_x}{l_x}, \frac{2\pi m_y}{l_y}\right), \quad (37)$$

where m_x and m_y are integers and l_x and l_y are the linear dimensions of the cortex, maps to the row or column index

$$\mu(a,m_x,m_y) = 1 + (m_x + M_{\max}) + (m_y + M_{\max})(2M_{\max}+1) + (a-1)(2M_{\max}+1)^2. \quad (38)$$

This index runs from 1 to $Y = N'(2M_{\max}+1)^2$ when a refers to a neural population, and from 1 to $Z = J(2M_{\max}+1)^2$ where it refers to a stimulus type.

Using Eq. (38) we can write Eq. (32) as

$$\sum_\nu A_{\mu\nu}Q_\nu = \sum_\zeta B_{\mu\zeta}N_\zeta, \quad (39)$$

or, more simply, as the matrix equation

$$\mathbf{AQ} = \mathbf{BN}, \quad (40)$$

where $\mathbf{A}$ is a $Y\times Y$ square matrix, $\mathbf{Q}$ is a $Y\times 1$ column matrix, $\mathbf{B}$ is a $Y\times Z$ rectangular matrix, and $\mathbf{N}$ is a $Z\times 1$ column matrix.

We can immediately invert Eq. (40) to find $\mathbf{Q}$ in terms of the stimuli $\mathbf{N}$:

$$\mathbf{Q} = \mathbf{TN}, \quad (41)$$

where $\mathbf{T} = \mathbf{A}^{-1}\mathbf{B}$ is the $Y\times Z$ rectangular transfer matrix of the system. The element T_{ab} is the response of Q_a at some $\mathbf{k}$ and ω to a change in N_b at the same frequency and some (possibly different) wave vector.

B. Observables

A measurable scalar quantity ψ (which could be a component of a vector) may well be able to be approximated by a linear combination of the Q_a (e.g., a scalp potential may involve contributions from several cellular populations, with various weights). In this case, at a given ω,

$$\psi(\omega) = \mathbf{MQ} = \mathbf{MTN}, \quad (42)$$

where $\mathbf{M}$ is a row vector of measurement coefficients, complex valued in general to include spatiotemporal filtering characteristics, phase shifts, etc.

Among key observables are the individual fields in $\mathbf{k}$ space or coordinate space. For example, the coefficients of the matrix $\mathbf{M}$ can be chosen such that

$$\psi(\omega) = \phi_{ab}(\mathbf{r},\omega) = \sum_{\mathbf{k}} \phi_{ab}(\mathbf{k},\omega)e^{i\mathbf{k}\cdot\mathbf{r}}. \quad (43)$$

Further classes of measurement functions are those relating the neural activity to local field potentials, multiunit activity,

the blood oxygen level dependent response that forms the basis of functional magnetic resonance imaging, or the metabolic responses underlying positron emission tomography, or single-photon emission computed tomography, for example.

In general, the use of a measurement matrix fits well with measurement and control theory. Use of a similar input matrix to relate raw stimuli to those that reach the brain would also enable preprocessing (e.g., retinal) of stimuli to be treated under the same formalism.

C. Dispersion and stability

The dispersion relation of linear waves in the system is given by

$$\det \mathbf{A}(\mathbf{k},\omega) = 0, \tag{44}$$

and the system is stable at a particular real $\mathbf{k}$ if all the frequency roots of this equation have negative imaginary part. If the steady state is stable for all $\mathbf{k}$, the spectra and other properties of the linear perturbations can be self-consistently defined.

D. Spectra

The power spectral density of ψ at $\mathbf{k}$ and ω is

$$P(\mathbf{k},\omega) = |\psi(\mathbf{k},\omega)|^2 = |\mathbf{M_k T N}|^2, \tag{45}$$

where $\mathbf{M_k}$ is defined so as to project out only the $\mathbf{k}$ component of ψ. The frequency and wave number spectra are then

$$P(\omega) = \int \frac{d^2\mathbf{k}}{(2\pi)^2} P(\mathbf{k},\omega), \tag{46}$$

$$P(\mathbf{k}) = \int \frac{d\omega}{2\pi} P(\mathbf{k},\omega). \tag{47}$$

A position-dependent spectrum can be calculated from Eq. (43).

V. APPLICATION TO THE CORTICOTHALAMIC SYSTEM

This section is devoted to an illustrative application to the corticothalamic system. We first improve the representation of propagators in the model of brain dynamics developed in our previous papers [10–12,15–17]. We then explore the spectral properties of the improved model, including the existence of an additional resonance in the gamma band (>30 Hz) when the improved propagators are introduced. In order to focus on the key propagator physics, we concentrate on signals at the cortical surface (electrocorticograms, or ECoGs); the effects of volume conduction must also be included when considering signals recorded at the scalp.

A. Improvement to propagators in a previous model

In previous studies we introduced a model of the cortex and thalamus, including separate cortical excitatory (e), mid-range excitatory (m), and short-range inhibitory (i) populations, plus both the reticular (subscript r) and specific relay (s) thalamic nuclei; we term this the EMIRS model for convenience. Figure 1 shows the connectivities in this model. Within the cortex, random connectivity was assumed, implying that all the gains G_{cb} are equal for fixed b, with c and c' denoting cortical populations (e, m, or i). We also assumed a common sigmoidal function.

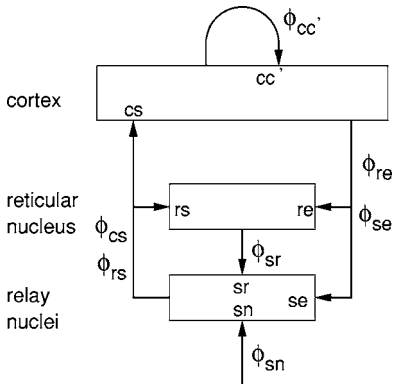

FIG. 1. Schematic of the connectivities in the model corticothalamic system used in Sec. V. The cortical populations ($c,c' = e,m,i$), reticular nucleus (r), and relay nuclei (s) are shown. Also shown are pulse-rate fields ϕ_{ab} that propagate from population b to population a, including external inputs ϕ_{sn}.

We illustrate the differences involved in introducing more general propagators via their effects on the linear EEG spectrum. Using the analysis in Secs. II and IV we calculate the matrices $\mathbf{A}$, $\mathbf{B}$, and $\mathbf{T}=\mathbf{A}^{-1}\mathbf{B}$. Selecting the element of $\mathbf{T}$ that relates ϕ_{ee} to the thalamic inputs ϕ_{sn} then yields the linear transfer function

$$\frac{\phi_{ee}(\mathbf{k},\omega)}{\phi_{sn}(\mathbf{k},\omega)} = \frac{K_{es}K_{sn}}{k^2 r_{ee}^2 + q_{0ee}^2 r_{ee}^2}[(1-K_{sr}K_{rs})(1-K_{ee}-K_{em}-K_{ei}) - K_{es}(K_{se}+K_{sr}K_{re})]^{-1}, \tag{48}$$

$$K_{ab} = K_{ab}(\mathbf{k},\omega) = J_{ab}(\omega)\Gamma_{ab}^{(0)}(\mathbf{k},\omega), \tag{49}$$

where Eq. (49) defines K_{ab} via Eqs. (16) and (26).

In the Appendix we estimate the parameters in this model, which are summarized in Table I. Using these parameters, we can make the following approximations for some of the propagators, provided $kr_{ab} \ll 1$ and $\omega \ll \gamma_{ab}$ in each case: $\Gamma_{ci}^{(0)} \approx 1$, $\Gamma_{cm}^{(0)} \approx 1$, and $\Gamma_{cs}^{(0)} \approx 1$ for all cortical components c, $\Gamma_{sr}^{(0)} \approx \Gamma_{rs}^{(0)} = 1$, and finally $\Gamma_{re}^{(0)} \approx \Gamma_{se}^{(0)} \approx 1$. In this regime in the absence of a mid-range population m, the main qualitative difference from previous work is that we cannot set $\Gamma_{se}^{(0)} = \Gamma_{ee}^{(0)}$, as was done implicitly before (the present result reproduces the previous one if this is done), since corticothalamic projections are more topographically localized than corticocortical ones [24,28]. The most significant quantitative differences from the previously used parameters (also summarized in Table I) are in the damping rates γ_{ei}, γ_{rs}, and γ_{sr}, which no longer greatly exceed the highest frequencies of interest in EEG and ECoG applications, ~100 Hz. In the next subsection, we show that γ_{ei} can have a significant effect on waves in the gamma frequency range (>30 Hz).

Using the above values for the propagators, we find

TABLE I. Illustrative brain parameters for normal adults in the alert, eyes-open state. The first column gives a brief description of the parameter, with its symbol listed in the second. The third and fourth columns give the estimates of the new parameters used in Sec. V and those used in previous studies, respectively, while the unit of each quantity is given in the final column. Only nonzero values for connections that are retained here are listed. All the r_{ab} and v_{ab} values are estimated for the visual system and are given in terms of dimensional map coordinate units and must be multiplied by the scale of the target structure relative to the cortex (0.1 for the human thalamus, as discussed in the Appendix) to obtain actual physical values. All the synaptodendritic rates have been assumed equal, regardless of a and b, and the index c denotes cortical populations e, m, i. The reason for sum $G_{cm}+G_{ci}$ appearing in the second column is that only the sum of these two quantities has been determined with reasonable accuracy in previous human studies. The quantities r_{cm}, v_{cm}, and γ_{cm} did not occur in the old version.

Quantity	Symbol	Estimate	Old	Unit
Propagation delays	τ_{re}, τ_{se}	43	43	ms
	τ_{cs}	43	43	ms
Synaptodendritic rates	α_{ab}	80	80	s^{-1}
	β_{ab}	800	800	s^{-1}
Gains	G_{ce}	6.8	6.8	
	$G_{cm}+G_{ci}$	−8.1	−8.1	
	G_{cs}	1.7	1.7	
	G_{re}	1.0	1.0	
	G_{rs}	0.19	0.19	
	G_{se}	2.5	2.5	
	G_{sr}	−1.9	−1.9	
	G_{sn}	0.8	0.8	
Projection ranges	r_{ce}	85	85	mm
	r_{cm}	2	n.a.	mm
	r_{ci}	0.2	0.3	mm
	r_{re}, r_{se}	1.2	85	mm
	r_{cs}	0.3	$\lesssim$0.3	mm
	r_{rs}	1.2	$\lesssim$0.3	mm
	r_{sr}	1.2	$\lesssim$0.3	mm
	r_{sn}	1.2	$\lesssim$0.3	mm
Projection velocities	v_{ce}	10	10	$m\,s^{-1}$
	v_{cm}	1	n.a.	$m\,s^{-1}$
	v_{ci}	0.3	10	$m\,s^{-1}$
	v_{re}, v_{se}	36	10	$m\,s^{-1}$
	v_{cs}	3.6	10	$m\,s^{-1}$
	v_{rs}	2	10	$m\,s^{-1}$
	v_{sr}	2	10	$m\,s^{-1}$
	v_{sn}	70	10	$m\,s^{-1}$
Damping rates	γ_{ce}	120	120	s^{-1}
	γ_{cm}	500	n.a.	s^{-1}
	γ_{ci}	1500	3×10^5	s^{-1}
	γ_{re}, γ_{se}	3×10^4	120	s^{-1}
	γ_{cs}	1.2×10^4	$\gtrsim3\times10^5$	s^{-1}
	γ_{rs}	1700	$\gtrsim3\times10^5$	s^{-1}
	γ_{sr}	1700	$\gtrsim3\times10^5$	s^{-1}
	γ_{sn}	6×10^5	$\gtrsim3\times10^5$	s^{-1}

$$\frac{\phi_{ee}(\mathbf{k},\omega)}{\phi_{sn}(\mathbf{k},\omega)} = \frac{J_{es}J_{sn}}{k^2r_{ee}^2+q_{ee}^2r_{ee}^2}\frac{1}{(1-J_{sr}J_{rs})(1-J_{em}-J_{ei})}, \tag{50}$$

$$q_{ee}^2r_{ee}^2 = (1-i\omega/\gamma_{ee})^2 - \frac{1}{1-J_{em}-J_{ei}} \times\left[J_{ee}+\frac{J_{es}(J_{se}+J_{sr}J_{re})\Gamma_{se}^{(0)}}{(1-J_{sr}J_{rs})\Gamma_{ee}^{(0)}}\right] \tag{51}$$

at low k, where the arguments of the J_{ab} have been omitted for compactness in Eqs. (50) and (51). In previous work $\Gamma_{ee}^{(0)}$ and $\Gamma_{es}^{(0)}$ canceled in the final term, leaving the only dependence on k to be that in the first denominator on the right in Eq. (50).

Equations (50) and (51) can be rearranged to isolate the terms that depend on k, which is useful when integrating over k to obtain quantities such as frequency spectra, since the integrals then have a simple form (integrals over ω can only be done in closed form in highly restrictive special cases). In the case where $\Gamma_{se}^{(0)}\approx1$, which is a reasonable approximation for small to moderate k, one finds

$$\frac{\phi_{ee}(\mathbf{k},\omega)}{\phi_{sn}(\mathbf{k},\omega)} = \frac{J_{es}J_{sn}}{k^2r_{ee}^2+p_{ee}^2r_{ee}^2}[(1-J_{sr}J_{rs})(1-J_{em}-J_{ei}) - J_{es}(J_{se}-J_{sr}J_{re})]^{-1}, \tag{52}$$

$$p_{ee}^2r_{ee}^2 = (1-i\omega/\gamma_{ee})^2 - \frac{J_{ee}}{1-J_{em}-J_{ei}-J_{es}(J_{se}+J_{sr}J_{re})/(1-J_{sr}J_{rs})}. \tag{53}$$

B. Spectra

Previous work has shown that the assumption of approximately white noise inputs to the corticothalamic system gives good agreement with a range of experimental data on EEGs and ECoGs, including spectra [10–13,15–19,21], which are predominantly generated by long-range excitatory neurons in the cortex [6,7,29]. Here we explore the spectral properties of our system on this assumption to probe the effects of the improved propagators.

Figure 2(a) shows the frequency spectrum $P_{ee}(f)$, where $f=\omega/2\pi$, estimated by integrating the squared modulus of Eq. (48) over $\mathbf{k}$ for the old parameters in Table I. As in previous work, the frequency spectrum shows the alpha and beta resonances, which are due to corticothalamic resonances near 10 and 20 Hz, respectively, in this theory [11,16]. There is a leveling off at low f, a $1/f$ spectrum at roughly 2–6 Hz,

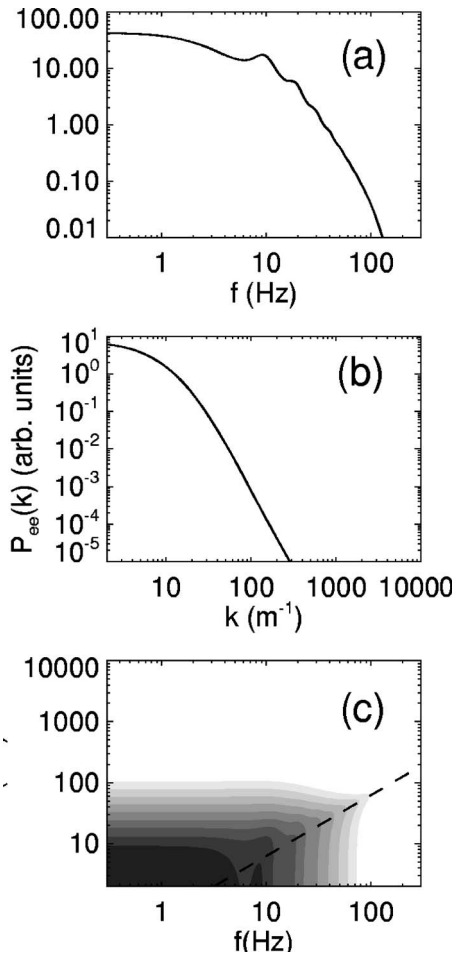

FIG. 2. Spectra of ϕ_{ee} obtained from the corticothalamic model with the old parameters from Table I and no m population. (a) Frequency spectrum $P_{ee}(f)$. (b) Wave number spectrum $P_{ee}(k)$. (c) Frequency–wave number spectrum $P_{ee}(f,k)$ with dark shading indicating high values, logarithmically spaced in half decades from a minimum of 10^{-6}. The curve $\omega=k_{vee}$ is shown dashed.

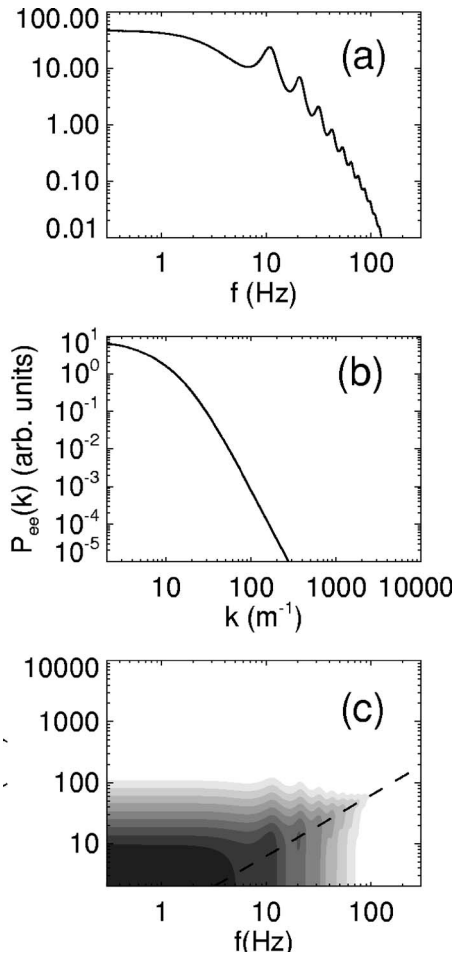

FIG. 3. Spectra of ϕ_{ee} for the old parameters from Table I, but the new r_{ab}, and no m population. (a) $P_{ee}(f)$. (b) $P_{ee}(k)$. (c) $P_{ee}(f,k)$ with shading as in Fig. 2 and dashes showing $\omega=kv_{ee}$.

and a steepening at high f, caused by the onset of synaptodendritic low-pass filtering [10,11,16]. The corresponding wave number spectrum falls off at $k \gtrsim 1/r_{ee}$, with a plateau developing below this point, also as found in previous work [18,19]. These aspects encapsulate key features of the combined frequency–wave number spectrum $P_{ee}(k,\omega)$ shown in Fig. 2(c), which also shows that the spectrum extends furthest along the line $\omega=kv_{ee}$, where damping is least [10]. Incidentally, the spectrum of the firing rate Q_e extends to much higher k because the first denominator on the right of Eq. (48) is absent in this case. This leads to obscuring of the spectral peaks in the corresponding frequency spectrum of Q_e. Hence, the reason that these peaks are visible in Fig. 2(a) is spatial filtering by long-range propagation (volume conduction would have a similar effect).

Figure 3 is analogous to Fig. 2, except that the new ranges r_{ab} have been included, from Table I (with the old velocities v_{ab}). This has the effect of sharpening the spectral peaks somewhat, chiefly because the smaller values of r_{se} and r_{re} make the corticothalamocortical connections more specific. Inspection of the corresponding spectra (not shown) for fields in the relay nuclei reveals that they are less concentrated at low k because of the shorter ranges of the corticothalamic input fibers.

Figure 4 has the same parameters as Fig. 2, except that the new velocities have been used (with the old ranges). This change leaves the frequency spectrum almost unaltered, apart from the appearance of an enhancement at around 80 Hz in the gamma range. There is a slight corresponding distortion at $k \approx 60$ m^{-1} in the k spectrum in Fig. 4(b), and a noticeable enhancement at these coordinates in the combined spectrum. Examination of other spectra shows a strong feature in the spectrum $P_{ei}(k,\omega)$, but nothing noticeable in the thalamic spectra, thereby indicating that this is a cortical phenomenon. We analyze it in the next section.

Figure 5 is plotted for the new ranges and velocities. We see both a strengthening of corticothalamic resonances, and the presence of the cortical gamma enhancement relative to Fig. 2. In interpreting Fig. 5 in conjunction with data, it is important to note that the parameters would need to be reoptimized slightly in each case to achieve the best possible match.

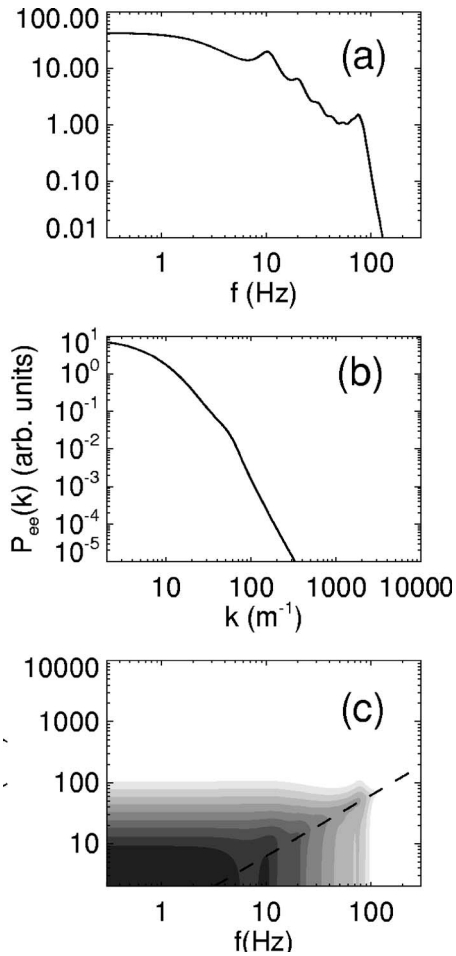

FIG. 4. Spectra of ϕ_{ee} for the old parameters from Table I, but the new v_{ab}, and no m population. (a) $P_{ee}(f)$. (b) $P_{ee}(k)$. (c) $P_{ee}(f,k)$ with shading as in Fig. 2 and dashes showing $\omega=kv_{ee}$.

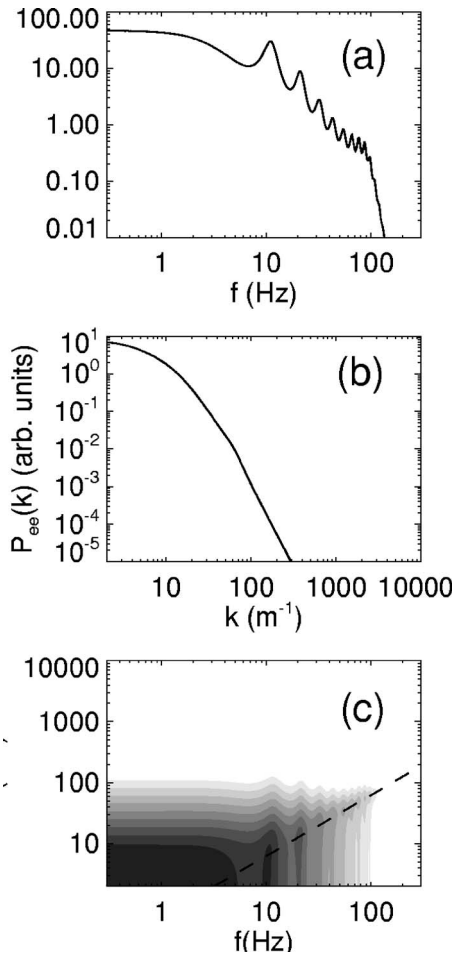

FIG. 5. Spectra of ϕ_{ee} for the new parameters from Table I and no m population. (a) $P_{ee}(f)$. (b) $P_{ee}(k)$. (c) $P_{ee}(f,k)$ with shading as in Fig. 2 and dashes showing $\omega=kv_{ee}$.

C. Gamma resonance

We next determine the nature of the gamma enhancement seen in Figs. 4 and 5. Filtering in the corticothalamocortical loops suppresses their effects in this frequency range, explaining the cortical nature of this phenomenon. If we ignore the thalamic terms in Eq. (48), the resonance in question proves to arise from a zero of the term $1-K_{ee}-K_{em}-K_{ei}$, involving relatively high k ($\gg 1/r_{ee}$) and ω. If we ignore the mid-range population for now (as in Figs. 2–5), note that $|K_{ee}| \ll |K_{ei}|$ at high k and ω, and assume that all the α_{ab} and β_{ab} are independent of a and b (which allows us to omit the subscripts on these quantities), the resonance underlying the gamma enhancement is determined by the equation $K_{ei}=1$, which is equivalent to

$$G_{ei} = (1 - i\omega/\alpha)(1 - i\omega/\beta)[k^2 r_{ei}^2 + (1 - i\omega/\gamma_{ei})^2]. \quad (54)$$

At marginal stability (i.e., exact resonance), the frequency and wave vector are real and the real and imaginary parts of Eq. (54) at moderate to low k (but not so low that K_{ee} must be retained) become

$$(1 - \omega^2/\alpha\beta)(1 - \omega^2/\gamma_{ei}^2) - 2\omega^2(\alpha + \beta)/\alpha\beta\gamma_{ei} = G_{ei}, \quad (55)$$

$$\omega[(\alpha + \beta)(1 - \omega^2/\gamma_{ei}^2)/\alpha\beta + (2/\gamma_{ei})(1 - \omega^2/\alpha\beta)] = 0, \quad (56)$$

respectively. One solution of Eq. (56) is at $\omega=0$, in which case Eq. (55) has the solution $G_{ei}=1$, which is unphysical, since G_{ei} is negative; in previous publications, an approximation equivalent to $\gamma_{ei}=\infty$ was made, which allowed only this unphysical solution. The other solution of Eq. (56) is

$$\omega^2 = \frac{\gamma_{ei}(2\alpha\beta + \alpha\gamma_{ei} + \beta\gamma_{ei})}{\alpha + \beta + 2\gamma_{ei}}, \quad (57)$$

which increases monotonically with α, β, and γ_{ei} and satisfies $\min\{\alpha, \gamma_{ei}\} \leqslant \omega \leqslant \max\{\beta, \gamma_{ei}\}$. Equations (55) and (57) yield

$$G_{ei} = -\frac{2(\alpha' + \beta')(1 + \alpha')^2(1 + \beta')^2}{\alpha'\beta'(\alpha' + \beta' + 2)^2}, \quad (58)$$

with $\alpha' = \alpha/\gamma_{ei}$ and $\beta' = \beta/\gamma_{ei}$. Equation (58) gives the value for exact resonance where Eq. (48) diverges. Such a resonance is possible only if $|G_{ei}|$ exceeds a critical value, below which there is a spectral enhancement at frequencies approximately given by Eq. (57). Symmetry of α' and β' in

Eq. (58) implies that this value lies where $\alpha' = \beta'$, whence it is easily shown that the minimum magnitude of the right side of Eq. (58) is 4, and this occurs when $\alpha = \beta = \gamma_{ei}$, giving $\omega = \alpha$. If $kr_{ei} \gg 1$, a similar analysis implies

$$\omega^2 = \alpha\beta, \tag{59}$$

$$G_{ei} = -(\alpha + \beta)^2 k^2 r_{ei}^2 / \alpha\beta, \tag{60}$$

which implies $|G_{ei}| \geqslant 4$ for exact resonance.

For the parameters in Table I, we predict resonance at $f = 120$ Hz and $G_{ei} = -16$ for $kr_{ei} \lesssim 1$, and at $f = 40$ Hz and $|G_{ei}| \geqslant 12$ in the opposite case. The cortical nature of the resonance and its approximate frequency accord with the results in Fig. 5(c). Agreement of the predictions with numerics is more easily seen in Fig. 6, where we show corresponding results for $G_{ei} = -16$ and the other parameters as in Table I (with no m population). The resonant frequency and critical gain agree well with the predictions (57) and (58) although the frequency downshift is truncated by low-pass filtering in k and is thus seen chiefly in the spectrum $P_{ei}(k, \omega)$ in Fig. 6(d). The latter feature leads to the appearance of a weak peak in $P(k)$ at $k \approx 60$ m^{-1} in Fig. 6(b). One further point is that the spectral enhancement actually extends to very small k, where K_{ee} cannot obviously be neglected; the analysis is thus more general than expected.

Spectral enhancements of cortical EEG activity in the 30–70 Hz gamma range have been widely observed in connection with perception [30]. It is thus of considerable interest to determine whether the resonance identified above could be responsible for these enhancements. Likely ranges $r_{ei} = 0.1$–0.3 mm and $v_{ei} = 0.1$–0.4 m s^{-1} imply $\gamma_{ei} = 330$–4000 s^{-1}. Together with likely waking ranges of $\alpha = 80 \pm 15$ s^{-1} and $\beta = 800 \pm 200$ s^{-1} [21], Eq. (57) implies a resonant frequency in the range 40–230 Hz, which overlaps most of the observed one.

The points raised in the above discussion are consistent with the resonance identified here being responsible for observed gamma enhancements, with one exception: intracellularly observed gamma oscillations often display fine structure down to scales of a few tenths of a millimeter ($k \gtrsim 6000$ m^{-1}) [30], whereas our spectra (even of Q_e, where spatial filtering cuts in strongly only at $k \gtrsim 3000$ m^{-1}) are very broad in k. This point remains to be resolved before any positive conclusion regarding the connection to gamma oscillations can be reached; however, we speculate that known mesoscopic structure at the relevant scales [7,24–26,30] may lead to stronger k dependence in the appropriate range.

Incidentally, intracortical resonances involving *ei* and *ii* loops (both subsumed under the *ei* subscripts here, via the random connectivity approximation) have been suggested as the mechanism underlying alpha activity at about 10 Hz. Leaving aside problems associated with the neglect of corticothalamic loops in such models, the above analysis leads to a requirement for unrealistically low waking values of α, β, and γ_{ei} (*all* less than 60 s^{-1}) for such mechanisms to be feasible.

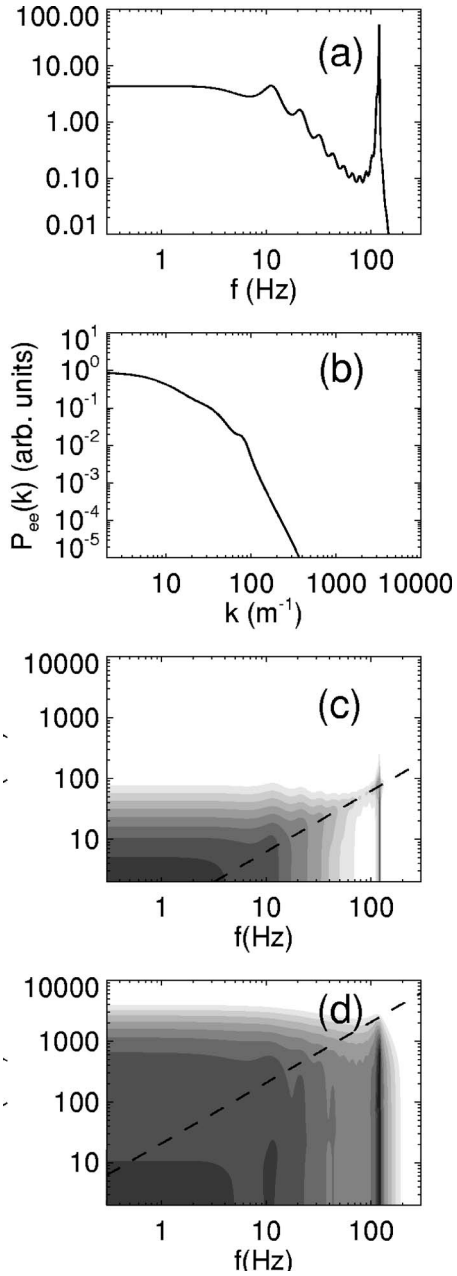

FIG. 6. Spectra of ϕ_{ee} and ϕ_{ei} for the new parameters from Table I, but $G_{ei} = -16$, and no m population. (a) $P_{ee}(f)$. (b) $P_{ee}(k)$. (c) $P_{ee}(f,k)$, with shading as in Fig. 2 and dashes showing $\omega = kv_{ee}$. (d) $P_{ei}(f,k)$ in the same format as (c), but with $\omega = kv_{ei}$ shown dashed.

D. Effects of intermediate-range cortical neurons

Figure 7 shows the effect of adding a mid-range population m of excitatory cortical neurons, with the parameters shown in Table I, with $G_{em} = 7.9$ and $G_{ei} = -16$ to keep the sum of these two gains equal to -8.1. Comparison with Fig. 5 shows a more prominent gamma enhancement in Fig. 7(a), due to the higher value of $|G_{ei}|$; this enhancement is also seen in Figs. 7(b) and 7(c). However, this is not as prominent as in Fig. 6 because the term K_{em} cannot be neglected in Eq. (48), and its gain factor has the opposite sign to the one in K_{ei} (if the two ranges were equal, there would be no change from

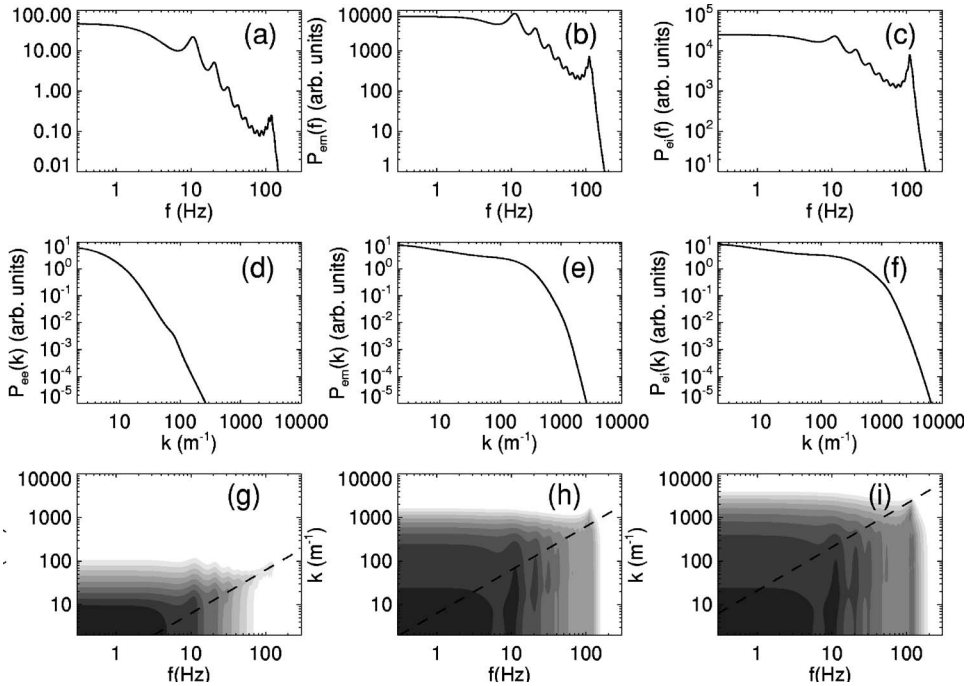

FIG. 7. Spectra of ϕ_{ee} for the new parameters from Table I, with $G_{em}=7.9$ and $G_{ei}=-16$. (a)–(c) Frequency spectra P_{ee}, P_{em}, and P_{ei}. (d)–(f) Wave number spectra P_{ee}, P_{em}, and P_{ei}. (g)–(i) Frequency–wave number spectra P_{ee}, P_{em}, and P_{ei}, with shading as in Fig. 2 and dashes showing $\omega = kv_{ee}$, $\omega = kv_{em}$, and $\omega = kv_{ei}$, respectively.

Fig. 5; if r_{em} were much greater than r_{ei}, K_{em} could be ignored and the situation would be as in Fig. 6). The wave number spectra in Figs. 7(d)–7(f) display characteristic cutoffs at the reciprocals of the respective axonal ranges [18,19], with weak low-k features in $P_{em}(k)$ and $P_{ei}(k)$ that result from driving by the e neurons. Figures 7(h) and 7(i) show a distinct, but weak, peak in the spectra $P_{em}(k,\omega)$ and $P_{ei}(k,\omega)$, but this feature is not seen in analogous spectra of Q_a (not shown). (Note that the spectra P_{ca} have the same form for all cortical populations c if a is fixed.) This implies some spatial structure corresponding to $k \approx 1000$ m^{-1} and $\omega \approx kv_{em}$ or $\omega = kv_{ei}$, respectively. For the correct combination of observed scale ($\sim$1 mm) and frequency ($\sim$40 Hz) to be achieved by this mechanism, one would require the relevant axonal velocity to be around 0.04 m s^{-1}, which is too low to be realistic [31].

VI. SUMMARY

A generalized, propagator-based, continuum treatment of brain dynamics has been developed, enabling arbitrary numbers of neural populations to be included, with distinct signal propagation characteristics between each pair of populations. Mesoscopic structure associated with neural arborization is included and widely converging or diverging projections can be treated. The predictions of the theory are expressed in terms of a moderate number of physiologically constrained parameters. The linear properties of the system have been explored for the case where underlying parameters are uniform across the brain.

As an illustrative application of the theory, it is used to improve treatment of signal propagation in a corticothalamic model that has been applied to explain a range of EEG and ECoG data in recent years. It is shown that more realistic corticothalamic propagators can lead to sharpening of the corticothalamic resonances that underly major brain rhythms, such as the alpha rhythm. More accurate analysis of corticocortical propagators can also lead to spectral enhancements in the gamma range, which arise from feedback loops involving slow, short-range, inhibitory fibers. Similar loops may occur in thalamic relay nuclei, which contain inhibitory interneurons in some species [28].

Physiologically realistic propagator parameters yield resonances in the observed gamma frequency range, but relatively broadly distributed in wave number, without the strong wave number structure that would account for observed spatial structure on scales of $\sim$1 mm for realistic axonal velocities. It is speculated that this structure may arise from well-known mesoscopic anatomical nonuniformities at this scale, which cannot be treated using uniform-medium propagators. It appears that the 10 Hz waking alpha rhythm cannot be generated by this mechanism for realistic parameter values. This is consistent with $\sim$15 Hz spindle generation during sleep via a related mechanism in the thalamus, because of the much lower values of α and β for the relevant neurotransmitters in that case [11,13,21].

Another area where the analysis developed here is applicable is treatment of the cortex as a multilayered structure (it has six main layers), rather than as a single layer with effective-medium properties, using different signal propagation characteristics to and from each layer. The effects of diffuse projection systems of the thalamus can also be studied, and incorporation of the basal ganglia, limbic system, brainstem, and other structures into modeling will be facilitated by the general formalism developed here.

ACKNOWLEDGMENTS

The author thanks C. J. Rennie for his helpful comments. The Australian Research Council supported this work.

APPENDIX: ESTIMATION OF PARAMETERS

In this appendix we estimate typical parameters for illustrative use in Sec. V, as summarized in Table I. More detailed analysis of the physiology would assign somewhat different individual values to many of these quantities, but the values in Table I suffice for illustrative purposes.

The first group of parameters in Table I are the mean propagation delays, synaptodendritic rates, and gains determined for 100 adult subjects in the waking eyes-open state by fitting the previous version of the model described in Sec. V A to EEG frequency spectra [21]. As discussed previously [12,18,19], because of its insensitivity to short spatial scales, this process does not distinguish the gains G_{cm} and G_{ci} separately, only their sum. (See Sec. V D for exploration of the balance between the two individual values.)

Of the projection ranges, the quantities r_{ce}, γ_{ce}, v_{ce}, $v_{se}=v_{re}=v_{cs}$ were also estimated in the above study [10], where c denotes a cortical population.

For present purposes we need to determine improved values of the other quantities listed in Table I. Beginning with the ranges, we note that values in the literature imply $r_{ci}\approx 0.2$ mm (this is a characteristic range of decrease in a single direction; the full width of an arbor would be about three times this value) with $r_{cm}\approx 2$ mm [24,27,28] at least for the visual cortex. Estimates of velocities are in the vicinity of $v_{ci}\approx 0.3$ and $v_{cm}\approx 1$ m s^{-1} [6,7,24,26,28,31].

Axonal arborization of thalamocortical fibers corresponds to a transverse characteristic distance of $r_{cs}=0.3$ mm [28], fanning out near the end of the axon. Hence, the characteristic time interval over which signals spread this far is $1/\gamma_{cs}\approx r_{cs}\sqrt{2}/V_{cs}$, where $V_{cs}\approx 5$ m s^{-1} is the physical velocity in the thalamocortical fibers (the factor of $\sqrt{2}$ assumes an approximately 45° opening half angle of the axonal tree where it arborizes). Writing $\gamma_{ab}=v_{ab}/r_{ab}$ in the usual way then yields the effective velocity $v_{cs}=3.6$ m s^{-1}. A similar calculation gives $v_{re}=v_{se}=36$ m s^{-1}, where the extra factor of 10 represents the ratio of cortical to thalamic scales: since all quantities are expressed in dimensional map units, thalamic distances, and velocities must be increased by this factor relative to their physical values. The ratio of 10 is estimated to be the square root of the ratio of cortical area (1500 cm^2 per hemisphere) to the combined cross sectional area of the nuclei in one-half of the thalamus ($\sim$15 nuclei at $\sim$1 cm^2 each). The values of the corticothalamic ranges $r_{re}=r_{se}$ are set to four times the corresponding thalamocortical ones, based on physiological estimates [28]; this is less than the relative scale factor because of somewhat less extensive physical arborization. The values of $\gamma_{re}\approx\gamma_{se}$ and $v_{re}\approx v_{se}$ in Table I are also estimated by the above methods.

Since intrathalamic fibers are not myelinated, we approximate their physical signal velocities by $v_{sr}\approx v_{rs}\approx 0.3$ m s^{-1}, as for the inhibitory cortical axons. We also assume a similar degree of arborization to corticothalamic axons. The methods above then lead to the corresponding velocities and damping coefficients listed in Table I.

Sensory input fibers are high velocity, so we choose the fiber velocity $v_{sn}=10$ m s^{-1}. If we again assume a similar degree of arborization to corticothalamic axons, we find the range, velocity, and damping coefficient values listed in Table I.

[1] H. R. Wilson and J. D. Cowan, Kybernetik **13**, 55 (1973).
[2] F. H. Lopes da Silva, A. Hoeks, H. Smits, and L. H. Zetterberg, Kybernetik **15**, 27 (1974).
[3] P. L. Nunez, IEEE Trans. Biomed. Eng. **21**, 473 (1974).
[4] W. J. Freeman, *Mass Action in the Nervous System* (Academic, New York, 1975).
[5] F. H. Lopes da Silva, J. E. Vos, J. Mooibroek, and A. van Rotterdam, Electroencephalogr. Clin. Neurophysiol. **50**, 449 (1980).
[6] P. L. Nunez, *Electric Fields of the Brain* (Oxford University Press, Oxford, 1981).
[7] P. L. Nunez, *Neocortical Dynamics and Human EEG Rhythms* (Oxford University Press, Oxford, 1995).
[8] J. J. Wright and D. T. J. Liley, Behav. Brain Sci. **19**, 285 (1996).
[9] V. K. Jirsa and H. Haken, Phys. Rev. Lett. **77**, 960 (1996).
[10] P. A. Robinson, C. J. Rennie, and J. J. Wright, Phys. Rev. E **56**, 826 (1997).
[11] P. A. Robinson, C. J. Rennie, and D. L. Rowe, Phys. Rev. E **65**, 041924 (2002).
[12] C. J. Rennie, P. A. Robinson, and J. J. Wright, Biol. Cybern. **86**, 457 (2002).
[13] P. A. Robinson, C. J. Rennie, D. L. Rowe, S. C. O'Connor, J. J. Wright, E. Gordon, and R. W. Whitehouse, Neuropsychopharmacology **28**, S74 (2003).
[14] P. A. Robinson, J. J. Wright, and C. J. Rennie, Phys. Rev. E **57**, 4578 (1998).
[15] C. J. Rennie, J. J. Wright, and P. A. Robinson, J. Theor. Biol. **205**, 17 (2000).
[16] P. A. Robinson, C. J. Rennie, J. J. Wright, H. Bahramali, E. Gordon, and D. L. Rowe, Phys. Rev. E **63**, 021903 (2001).
[17] P. A. Robinson, R. W. Whitehouse, and C. J. Rennie, Phys. Rev. E **68**, 021922 (2003).
[18] S. C. O'Connor, P. A. Robinson, and A. K. I. Chiang, Phys. Rev. E **66**, 061905 (2002).
[19] S. C. O'Connor and P. A. Robinson, Phys. Rev. E **67**, 051912 (2003).
[20] P. A. Robinson, J. Theor. Biol. **222**, 163 (2003).
[21] P. A. Robinson, C. J. Rennie, D. L. Rowe, and S. C. O'Connor, Hum. Brain Mapp **23**, 53 (2004).
[22] D. L. Rowe, P. A. Robinson, and C. J. Rennie, J. Theor. Biol. **231**, 413 (2004).
[23] D. L. Rowe, P. A. Robinson, A. W. Harris, K. L. Felmingham, I. L. Lazzaro, and E. Gordon, J. Integrative Neurosci. **3**, 453 (2004).
[24] *Principles of Neural Science*, 3rd ed., edited by E. R. Kandel, J. H. Schwartz, and T. M. Jessell (Appleton and Lange, Norwalk, CT, 1991).
[25] P. Dayan and L. F. Abbott, *Theoretical Neuroscience* (MIT Press, Cambridge, 2001).

[26] C. Koch, *Biophysics of Computation* (Oxford University Press, Oxford, 1999).
[27] A. Destexhe, and T. J. Sejnowski, *Thalamocortical Assemblies* (Oxford University Press, Oxford, 2001).
[28] M. Steriade, E. G. Jones, and D. A. McCormick, *Thalamus* (Elsevier, Amsterdam, 1997).
[29] E. Niedermeyer and F. H. Lopes da Silva, *Electroencephalography: Basic Principles, Clinical Applications, and Related Fields*, 4th ed. (Williams and Wilkins, Baltimore, 1999).
[30] A. K. Engel, P. R. Roelfsma, P. Fries, M. Brecht, and W. Singer, Cereb. Cortex **7**, 571 (1997).
[31] H. Swadlow, in *Time and the Brain, Conceptual Advances in Brain Research*, edited by R. Miller (Harwood, Amsterdam, 2000), p. 131.